

Chapter 19

Magnetic Manipulation of Colloidal Particles

Randall M. Erb and Benjamin B. Yellen

Abstract We review some recent advances in the field of magnetic manipulation techniques, with particular emphasis on the manipulation of mixed suspensions of magnetic and nonmagnetic colloidal particles. We will first discuss the theoretical framework for describing magnetic forces exerted on particles within fluid suspensions. We will then make a distinction between particle systems that are highly dependent upon Brownian influence and those that are deterministic. In both cases, we will discuss the type of structures which are observed in colloidal suspensions as a function of the size and type of particles in the fluid. We will discuss the theoretical issues that apply to modeling the behavior of these systems, and we will show that the recently developed theoretical models correlate strongly with the presented experimental work. This chapter will conclude with an overview of the potential applications of these magnetic manipulation techniques.

19.1 Introduction

The manipulation of particle suspensions is an essential capability for various engineering applications ranging from self-assembled nano-manufacturing to life science analysis tools. Methods for manipulating the particles in parallel have mainly relied on the use of optical [1, 2], electrical [3, 4], or magnetic field traps [5–10], which have the advantage of being shaped remotely through the use of lasers, electrodes, or external coils. Magnetic manipulation techniques, in particular, have the practical advantage of being biologically and chemically invisible [11], as compared to electrical and optical systems which are prone to overheating or chemically altering the specimen [12, 13]. There are several comprehensive reviews in the literature

Benjamin B. Yellen (✉)

Department of Mechanical Engineering and Materials Science, Center for Biologically Inspired Materials and Material Systems, Hudson Hall, Box 90300, Duke University, Durham, NC 27708, USA

e-mail: yellen@duke.edu

describing developments in the field of magnetic manipulation systems over the last four decades [14–17]. This chapter will instead focus on the interesting capabilities that have recently been demonstrated in mixed magnetic and nonmagnetic particle suspensions, and we will emphasize our own recent advances in controlling particles of various sizes, shapes, and degrees of magnetization. Due to the inherent complexity in modeling systems composed of strongly interacting particles, this topic poses considerable theoretical and experimental challenges; however, we will show that continuum models can be effective at describing the equilibrium behavior of colloidal suspensions exposed to external magnetic fields.

The most common use of magnetic particles is in the field of separation, where magnetic manipulation schemes are applied to capture and separate various biological materials of interest (e.g., cells [18, 19], viruses [20, 21], and proteins [22, 23]). For magnetic separation applications, magnetic particle surfaces are typically functionalized with proteins and antibody receptors that can recognize and associate with various biological materials by affinity binding. Once attached, the biological materials are separated from solution by applying force to the magnetic particle. Consequently, there has been much effort in the synthesis and characterization of these colloidal magnetic particles, reviewed elsewhere [24].

Recently, we have demonstrated an alternative method for separating and manipulating biological and other nonmagnetic materials using a suspension of magnetic nanoparticles to provide “magnetic contrast” to the surrounding fluid. Nonmagnetic materials immersed within the suspension of magnetic nanoparticles are shown to become effectively magnetized with respect to the surrounding fluid, allowing them to be manipulated by magnetic fields and field gradients [6,7, 25–28]. This manipulation strategy has been given the name negative magnetophoresis in order to draw parallels with the corollary “negative dielectrophoresis” commonly referred to in the literature [29, 30].

The theoretical analysis of magnetic nanoparticle suspensions poses considerable challenges with respect to accurately calculating the magnetic force on submerged nonmagnetic materials. Compared with negative dielectrophoresis where continuum equations are generally applicable due to the solvent being much smaller than most colloidal materials, the analysis of magnetic nanoparticle suspensions is complicated by the larger size of the magnetic nanoparticles (~ 10 nm) which is commensurate with the size of many proteins and macromolecules. Furthermore, the strong interactions between 10 nm sized magnetic nanoparticles lead to a phenomenon (e.g., chaining), which is not observed in corollary dielectric systems where the solvent is of molecular length scale [31–33]. Larger particle size brings into question the applicability of continuum equations for fluid magnetization when considering nonmagnetic particles that are only slightly larger than the magnetic nanoparticles in the fluid. By investigating the agreement between theory and experiment, we show continuum models are applicable when the nonmagnetic particles are at least 2–3 times larger than the magnetic nanoparticles [10, 28].

The rest of this work will be organized as follows. In Section 19.2, we will introduce the theoretical basis of controlling magnetic and nonmagnetic particles and establish the role that is played by Brownian motion. In Section 19.3, we will

review some non-Brownian particle manipulation systems including surface-based assemblies and substrate-based transport. In Section 19.4, we will present magnetic and nonmagnetic particle systems where the manipulation of individual particles is influenced, but not dominated, by Brownian motion, such as chain growth, self-organizing structures, and the alignment of anisotropic particles. In Section 19.5, we will expand these models to account for the behavior within populations of nanoparticles which are dominated by Brownian fluctuations and must be modeled using Boltzmann distributions. We will demonstrate the validity of our theoretical predictions by comparing theoretical models with experimental results. In Section 19.6, we will conclude this discussion by outlining open questions and future directions for this field.

19.2 Magnetic Manipulation of Particles

19.2.1 Deterministic and Brownian-Dominated Particle Systems

Throughout this chapter, we will be discussing either particles which follow deterministic trajectories or ones dominated by random Brownian motion. The general principle of Brownian motion suggests that the positions of particles will fluctuate due to random collisions with the solvent molecules [34]. Owing to its smaller mass, the fluctuations of nanoparticles (i.e., <100 nm) tends to be much larger than microparticles; however, the Brownian interactions can be overlooked in some cases where the magnetic forces are particularly strong. In either case, it is worthwhile to establish a general guideline for when a particle's motion can be modeled deterministically and when random motions must be taken into account. Under an applied force, \vec{F}_p , a particle will experience a change of potential energy of $\Delta U(\vec{r}) = \vec{F}_p(\vec{r}) dr$. In this work, the particle's trajectory is considered to be deterministic when the change in potential energy during its movement over a distance commensurate with its own radius, a , is larger than thermal fluctuation energy (i.e., $2aF \geq k_B T$). If the change in potential energy is smaller than thermal fluctuation energy, then random Brownian motion cannot be ignored. To make this distinction for each type of motion, it is first necessary to discuss how to calculate magnetic forces on colloidal particles.

19.2.2 Material Properties

Before embarking on a discussion concerning the calculation of different forces, we first review the type of magnetic materials used in magnetic manipulation technology and their field-dependent behavior. Magnetic particles are typically composed of iron, nickel, or cobalt, and their various oxidized forms. A division in nomenclature is used to distinguish between the different types of magnetic ordering of spins within these materials. Iron, nickel, and cobalt in pure metal form are referred to

as ferromagnets, whereas their oxidized forms are referred to as ferrimagnets. For more discussion, see Ref. [35] or other chapters in this handbook. Regardless of these differences, both types of material classes display common magnetic properties, including the ability to store magnetization in the absence of external field (i.e., remanence), and a history-dependent magnetization (i.e., hysteresis). The hysteretic magnetization behavior of typical ferro/ferrimagnetic material below the Curie temperature is presented in Fig. 19.1A [35, 36].

When ferro/ferrimagnetic materials are heated above the Curie temperature, the spin–spin coupling within the material is no longer sufficient to overcome thermal fluctuation energy, and as a result these materials begin to display different behavior referred to as *paramagnetism*, which is characterized by a lack of remanence and hysteresis. In other words, paramagnetic materials can magnetize in an external field, but they promptly lose their magnetization when the field is removed. The classic paramagnetic hysteresis graph is shown in Fig. 19.1B, and the linear region is called the magnetic susceptibility, χ , which describes how easily the material can magnetize in an external field.

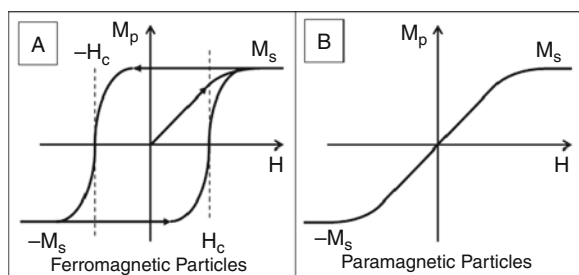


Fig. 19.1 Hysteresis curves for (A) ferromagnetic and (B) paramagnetic material. The magnetization, \bar{M}_p , of the particles increases with an applied field, \bar{H} , until the saturation magnetization, M_s , of the particle is reached. Ferromagnetic particles retain a magnetization in zero field that can only be switched in a reversal field exceeding the coercive field, H_c .

Recently, the term “superparamagnetism” has been given to a class of very small metal or metal-oxide nanoparticles (usually smaller than 10 nm) that display extraordinarily large paramagnetic response to an external field even at temperatures below the Curie point, where the bulk material would have magnetic remanence. This behavior originates from the competition between the nanoparticle’s magnetic crystalline anisotropy energy and the thermal fluctuation energy of the surrounding bath. Since the crystalline anisotropy energy is proportional to the volume of the nanoparticle, there exists a critical size below which the particles cannot retain its preferred magnetization orientation inside the material’s crystalline structure. This “superparamagnetic limit” is of particular interest to magnetic data storage technology, since it dictates the smallest nanoparticle that can store binary data. These materials are also of interest as magnetic nanoparticle fluids, since they remain stable in the absence of magnetic field but respond strongly when external field is applied.

In the last few decades, there have been significant advances in synthesizing fluidic suspensions of magnetic particles for various applications in drug delivery, cell, and molecular separation, and a variety of other applications [14]. One type of suspension, referred to as *magnetorheological fluid*, consists of 100 nm to 10 μm sized *magnetic beads* suspended in nonmagnetic carrier fluid. These magnetic beads are typically composed of a spherical polymer matrix which encapsulates a dispersion of magnetic nanoparticle grains. If the magnetic grains are small enough and spaced sufficiently far apart inside the polymer matrix, then the composite particle will behave superparamagnetically yet it will have a large dipole moment due to the collective response of the large number of magnetic grains inside the bead. The magnetic susceptibility of these commercially available beads is typically in the range of 0.1–1.0.

Another type of suspension, referred to as *ferrofluid*, consists of 5–20 nm sized magnetic nanoparticles that are freely suspended inside a nonmagnetic carrier fluid. The magnetic properties of the fluid can be modeled as a continuum when the fluid volume element under consideration is much larger than the individual nanoparticles. In our work, for example, we have found that ferrofluids having at least 0.1% volume fraction of magnetic nanoparticle material will behave as a magnetic continuum on the 100 nm length scale [64]. These fluids can also be characterized by a magnetic susceptibility which can be tuned by changing the concentration of nanoparticles within the fluid.

It is interesting to note that in some ferrofluids the overall fluid magnetization can display superparamagnetic properties despite its being composed of nanoparticles that are larger than the superparamagnetic limit. The mechanism for achieving superparamagnetic behavior is due to the Brownian rotational diffusion of the nanoparticles, as opposed to through the classic Neel mechanism (i.e., rotation of the magnetic moment inside the crystalline structure) [35]. For these fluids to remain stable, the nanoparticle cannot be too large, since force interactions between the ferro/ferrimagnetic nanoparticles can lead to irreversible aggregation. In most cases, ferro/ferromagnetic nanoparticles smaller than about 20 nm will remain colloidally stable, since thermal fluctuations will dominate not only the particle–particle magnetic force interactions but also other surface forces of relevance to this size scale. Thus, the criteria for modeling a medium as superparamagnetic must consider not only the properties of the material itself but also the mobility of particles inside their host matrix.

Finally, it is important to mention the role of shape in the particle magnetization process, which is commonly referred to as the “shape anisotropy” of the material. The magnetization of various particle shapes can be modeled using discrete dipole approximation techniques [36]. When the particle shapes conform to certain symmetrical geometries (e.g., spherical and ellipsoidal), these calculations can often be simplified with analytical functions at negligible cost to accuracy. Simplified models are especially beneficial for treating spherical particles, which are the most abundant particle geometry [35–37], and are unique in that the particle’s field is identical to a point dipole when it is uniformly magnetized. However, some corrections may be needed when the particle shape is slightly irregular or if the particle’s magnetization

is not uniform due to the presence of nearby magnetic sources [36, 38] (e.g., a permanent magnet or another particle). Numerical techniques can achieve better accuracy; however, the gains in improved accuracy are relatively minor and frequently not worth the computational investment [27] when applied to applications in magnetic separation and manipulation.

19.2.3 Magnetic Force

The stability of any colloidal suspension is highly dependent upon short-range forces (e.g., steric, Van der Waals, and depletion); however, particle trajectories are dominated by long-range forces (e.g., electrical, gravitational, and magnetic) [39, 40]. Electrical forces often exist in suspensions in the form of electric surface charges, which assist in stabilizing the suspension by repelling neighboring particles. These charges, however, will negligibly affect particle motion in dilute suspensions which are not exposed to electric fields. Gravitational forces can also be ignored for small magnetic particle suspensions over short-time scales [44]. Hence for the magnetic particle systems discussed in the following sections, we have neglected other forces entirely and have focused on the formation of colloidal structures solely due to magnetic forces.

The magnetic force on particles can be computed by considering the equivalent magnetic poles distributed inside the particle volume and on the particle surface. In the case of uniform magnetization, the magnetic poles are strictly on the particle's surface, and the equivalent magnetic pole density can be determined from the divergence in the normal component of magnetization at the particle surface, $\sigma = \mu_o (\vec{M}_p - \vec{M}_f) \cdot \hat{n}$, where \vec{M}_p and \vec{M}_f are the respective magnetizations of the particle and the surrounding fluid, and \hat{n} is the normal surface vector of the particle, S_p . The constant μ_o represents the magnetic permeability of free space, $\mu_o = 4\pi \cdot 10^{-7}$ [H/m]. The magnetic force, \vec{F}_p , that acts upon these magnetic poles is defined by

$$\vec{F}_p \equiv \iint_{S_p} \sigma \vec{H} dS = \mu_o \iint_{S_p} (\vec{M}_p - \vec{M}_f) \cdot \hat{n} \vec{H} dS \quad (19.1)$$

\vec{H} is the local magnetic field using SI notation where the magnetic flux density, \vec{B} , is related to the magnetization and local field by $\vec{B} = \mu_o (\vec{H} + \vec{M})$. Applying Gauss divergence theorem [14, 41], Eq. (19.1) can be reduced for a spherical particle of volume V_p to

$$\vec{F}_p \equiv \mu_o V_p \left[(\vec{M}_p - \vec{M}_f) \cdot \nabla \right] \vec{H} \quad (19.2)$$

Equation (19.2) indicates that in order to achieve significant magnetic force, the particles should have large volumes, there should be a large contrast between the magnetization of the particle and the fluid, and the manipulation system should

be capable of applying large magnetic field gradients. Equation (19.2) also indicates that both magnetic and nonmagnetic particles can be magnetically manipulated depending on the fluid magnetization. For example, magnetic microparticles surrounded by water, for which $\vec{M}_f = 0$, can experience large magnetic forces as evidenced by the numerous applications in magnetic manipulation [14], detection [42], and separation [8]. In weak magnetic fields where $M_p \ll M_s$, the particle magnetization follows a linear constitutive relationship $\vec{M}_p = \chi \vec{H}$, where χ is the bulk material susceptibility, as shown in Fig. 19.1B. This relationship allows the force to be expressed as

$$\vec{F}_p = \mu_o V_p (\vec{M}_p \cdot \nabla) \vec{H} = \frac{1}{2} \mu_o V_p \bar{\chi} \nabla \vec{H}^2 \quad (19.3)$$

where $\bar{\chi}$ is the susceptibility of the particle. The geometry of the particle also affects its ability to magnetize in an external magnetic field [43]; for example, spherical particles have a shape corrected susceptibility of $\bar{\chi} = 3\chi/(\chi + 3)$.

Magnetic force can also be applied to nonmagnetic particles provided the surrounding fluid has nonzero magnetization, such as ferrofluid. It is convenient to represent the fluid magnetization using continuum models, and this assumption tends to be reasonably accurate in cases when the fluid volume of consideration is much larger than the individual ferrofluid particles. An alternative method for modeling these suspensions would consist of considering each particle as a discrete dipole and using Monte Carlo techniques [44, 45] to track the average position and density of particles over time. Due to its computational complexity, these techniques are only applied by a limited number of groups, while most advances have employed continuum approximations. The force on a relatively large nonmagnetic particle (i.e., >50 nm) immersed in ferrofluid can be rewritten as

$$\vec{F}_p = -\mu_o V_p \left(\left\langle \vec{M}_f \right\rangle \cdot \nabla \right) \vec{H} \quad (19.4)$$

The effective fluid magnetization is a function of the magnetization of the individual magnetic particles, $\vec{M}_{p,m}$, and their volume fraction, C_m , as $\left\langle \vec{M}_f \right\rangle = \vec{M}_{p,m} C_m$. For very low magnetic fields where $M_{p,m} \ll M_s$, a linear constitutive relationship can be employed to describe the magnetization of the individual magnetic particles as $\vec{M}_{p,m} = \chi \vec{F}$. However, in strong magnetic field, the particle magnetization is more accurately characterized by Langevin's function, $L(x) = \coth(x) - x^{-1}$, which provides a mechanism to describe magnetization saturation [46], given by

$$\left\langle \vec{M}_f \right\rangle = \vec{M}_{p,m} C_m = M_s C_m L(\xi) \hat{H} \quad (19.5)$$

where ξ is a dimensionless ratio between the magnetic and thermal energy as $\xi = \mu_o M_{s,m} V_m |\vec{H}| / k_B T$, where V_m is the volume of the individual magnetic particles that comprise the ferrofluid. Combining Eq. (19.5) with Eq. (19.4) yields the force on nonmagnetic particles submerged in ferrofluid and subjected to magnetic field gradients as:

$$\vec{F}_p = -V_p M_s C_m L(\xi) (\hat{H} \cdot \nabla) \vec{H} = -k_B T C_m L(\xi) \nabla \xi \quad (19.6)$$

Thus, Eqs. (19.3) and (19.6) represent the forces experienced by magnetic particles surrounded by nonmagnetic carrier fluid, such as water, and by nonmagnetic particles surrounded by ferrofluid, respectively. These expressions will be applied to describe magnetic manipulation techniques in various colloidal particle systems and elucidate the role of magnetic force played in forming colloidal particle chains and other self-organizing structures, controlling alignment of anisotropically shaped colloidal particle, as well as the transport and assembly of colloidal particles onto magnetically patterned surfaces.

19.3 Deterministic Particle Manipulation

19.3.1 Substrate-Based Self-Assembly of Particles

In this section, we begin by discussing microfluidic systems in which the motion of colloidal particles is dominated everywhere by magnetic force. Brownian diffusion is assumed to play a negligible role, and thus the trajectory of particles will be calculated solely from the magnetic force and the viscous response of the environment. One example type of system is a magnetically patterned surface, containing an array of closely spaced magnets which produce both strong local field and field gradients, leading to magnetic forces exceeding piconewton strength on nearby colloidal particles. These types of magnetic separation systems can be fabricated by various lithographic techniques and have been studied by a number of researchers for applications in biochip technologies, manufacturing, and purification [8, 16, 46].

In some instances, the magnetic templates or islands are fabricated from ferromagnetic material that allow for magnetic information to be stored in the substrate and used to program the particle assembly instructions [47]. This programmability allows for the controlled placement of magnetic or nonmagnetic particles into desired regions of the substrate. For a particle near an island, the classical dipole field pattern for an island is shown in Fig. 19.2 superimposed on the uniform field. Without external fields, the field of the island, \vec{H}_{island} , will remain symmetric, having maxima of equal magnitudes near both magnetic poles and minima far away from the island; however, when an external field bias is applied to the system it is possible to change the locations of magnetic field maxima and minima.

As seen in Fig. 19.2, the magnitude of the local field can be altered by applying an external field, \vec{H}_o , such that the external field adds to the island's field in some locations and subtracts in other locations. In this particular example, \vec{H}_o adds to the magnitude \vec{H} on the right side of the island and reduces \vec{H} on the left, creating a field maximum and minimum, respectively. Thus, magnetic particles will be forced toward the right side of the island while nonmagnetic particles in ferrofluid will be forced to the left side. Because photolithographic patterning techniques are well developed, a magnetic template with a controllable field distribution is a very

straightforward method to create self-assembled arrays of particles onto specific locations of a surface.

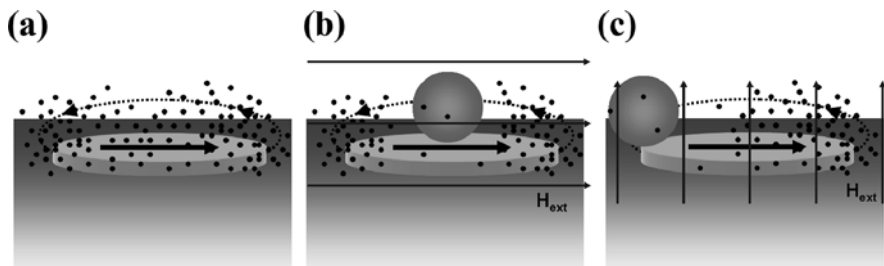


Fig. 19.2 Schematic illustration of nonmagnetic particle immersed in ferrofluid assembling on top of a micromagnet (grey disc with arrow denoting the island's magnetization). (A) Under no external field, the ferrofluid accumulates near the island, whereas the particle is forced away from the island toward the region of lower magnetic field. (B) The external magnetic field is applied parallel to the island's magnetization, causing the ferrofluid to accumulate around the edges of the island where the external field adds to the island's field (denoted by dotted line with arrow), meanwhile the nonmagnetic particle is pulled directly on top of the island where the external field subtracts from the island's field. (C) The external field is applied in the vertical direction that causes the nonmagnetic particle to move to the left edge of the island and the magnetic nanoparticles are pulled toward the right edge

19.3.2 Substrate-Based Transport and Separation

Time-varying magnetic fields applied to substrates of magnetic islands provide a new class of interesting physical behavior with potential ramifications in the transport and separation of colloidal particles. For example, a rotating external field applied to the system will move the locations of magnetic minima and maxima across the surface of the substrate. The transverse motion of these maxima and minima can be modeled as a traveling wave, as shown in Fig. 19.3, which transports individual particles horizontally across the substrate [8].

A simplified analytical model can be developed to model the particle's motion in response to a traveling wave. In this system, a rectangular array of circular magnetic islands patterned from thin ferromagnetic film will have an effective magnetic pole density on the array surface which is well approximated by a 1-D Fourier expansion. For the purpose of this analysis, we will still assume that the substrate's field can still be accurately modeled if only the first harmonic in the Fourier expansion is retained [48]. The sinusoidal pole distribution has an amplitude equal to the island's average pole density, σ_o , with the minimum and maximum of the sinusoid corresponding with the left and right side, respectively, of the island. In addition to the static field produced by the substrate, a spatially uniform rotating field is assumed to be applied to the substrate with frequency, ω . The total magnetic field will be the superposition of the island's field and the external field, and it will depend upon the particle radius, a , the periodicity of the island array, d , and time t , as

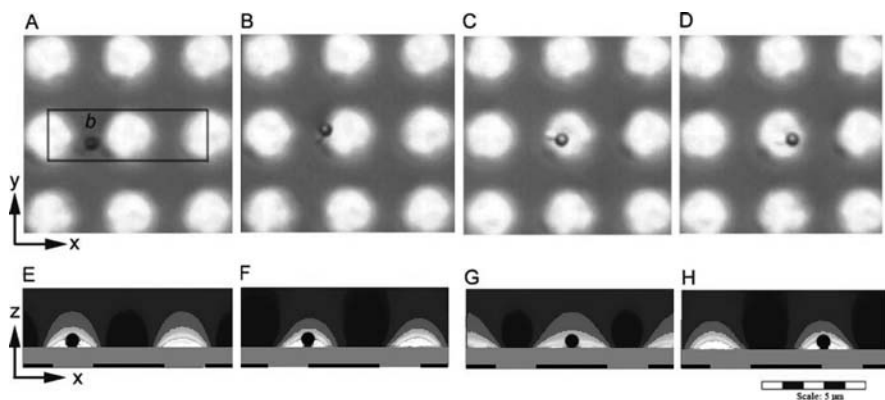


Fig. 19.3 (A–D) A magnetic label attached to a large virus transverse a magnetic array (magnetized in the + x direction) in the presence of a rotating field (also directed in the + x direction in (A) and rotating counterclockwise). (E–G) A finite element analysis of the magnetic array shows the magnetic field maxima (white) moving across the array with the rotating field. *Reproduced by permission of The Royal Society of Chemistry* [8]

$$\vec{H}_x = \vec{H}_{island,x} + \vec{H}_{o,x} = \frac{\sigma_o}{2} e^{-2\pi a/d} \sin\left(\frac{2\pi}{d}x\right) + H_o \sin(\omega t) \quad (19.7)$$

Thus, the force on a particle will be dependent upon the current position and time as $F_x = F_{p,x} \sin(2\pi x/d - \omega t)$, where $F_{p,x}$ can be input from either Eq. (19.3) or Eq. (19.6) depending on the type of system considered. The particle trajectory can be modeled from the equations of motion:

$$F_{net} = m \frac{d^2x}{dt^2} = F_x - D \frac{dx}{dt} \quad (19.8)$$

where m is the mass of the particle, and D is the viscous drag coefficient. In low Reynold's number flow, the inertial term can be ignored, thus the magnetic force is found to exactly balance the drag force on the particle, assumed in this case to be Stokes' drag on a sphere. It is convenient to write Eq. (19.8) in dimensionless form as

$$\frac{d\phi}{d\tau} = \sin(\phi) - \frac{\omega}{\omega_c} \quad (19.9)$$

where $\phi = 2\pi x/d - \omega t$, $\omega_c = 2\pi F_p/(dD)$ is a particle's critical frequency, and $\tau = \omega_c t$ is the dimensionless time variable. This equation of motion is similar to a nonlinear harmonic oscillator observed in many physical systems [49–51]. The behavior of a nonlinear harmonic oscillator suggests that two regimes of motion may be observed depending on the velocity of the traveling wave. If the traveling wave is moving too rapidly, then the substrate cannot supply enough magnetic force to maintain the particle's relative position within the traveling wave. On the

other hand, when the traveling wave is moving less rapidly, the particle becomes locked into the traveling wave and can move linearly across the substrate at a constant rate. Mathematically, this behavior is described as follows. When the system is below the critical frequency, Eq. (19.9) has a stable solution, and the velocity of the particle is found to be independent of drag forces as $dx/dt = \omega d / (2\pi)$. However, when the frequency exceeds ω_c , the viscous drag forces cause the particle to slip from the moving field maxima and reduce the particles linear velocity by $dx/dt = \left(\omega - \sqrt{\omega^2 - \omega_c^2} \right) d / (2\pi)$.

For simple transport systems, maintaining the rotating field below the critical frequency (i.e., $\omega < \omega_c$) can produce very reliable particle trajectories; however, the ability to separate magnetic particles of different sizes can be accomplished by adjusting the frequency close to or exceeding the critical frequency of the system (i.e., $\omega > \omega_c$). For most colloidal transport systems, the damping of the particle velocity is due solely from a Stokes' drag force of $F_{d,x} = 6\pi\eta a (dx/dt)$, where η is the viscosity of the fluid. The critical frequency can then be solved for as a function of a particle's susceptibility and radius:

$$\omega_c = \frac{\bar{\chi}\mu_o\sigma_o H_o}{18\eta} \left(\frac{2\pi a}{d} \right)^2 e^{-2\pi a/d} \quad (19.10)$$

From the dependencies of this equation, the transport velocity of particles with different size and susceptibility has a different frequency response. Exploiting this nonlinearity, the frequency of the rotating field can be adjusted to allow particles of certain size or magnetization to move freely while the motion of others is greatly impeded. For example, 3 μm magnetic particles have higher critical frequencies than similar 1 μm magnetic particles, shown in Fig. 19.4, which allows for their separation. Another separation system involves attaching bio-particles to magnetic particles, effectively reducing the magnetization of any reacted magnetic particle [8]. Then free magnetic particles could be separated quickly from the suspension, and any left over magnetic particles, those attached to the bio-particles, could be subsequently transported elsewhere on the chip (possibly for detection, extraction, or further analysis) by reducing the frequency of the rotating field.

19.4 Brownian-Influenced Particle Manipulation

19.4.1 Magnetic and Nonmagnetic Particle Chains

The motion of large magnetic beads is not always dominated by magnetic force. There may be regions in the fluid where relatively weak magnetic force is experienced by the particle, in which case its trajectory is dominated completely by random Brownian motion. However, when other particles are present in the fluid, the Brownian diffusion does not play a lasting role as particle–particle interactions begin to dominate. Here, we review some of the interesting particle–particle

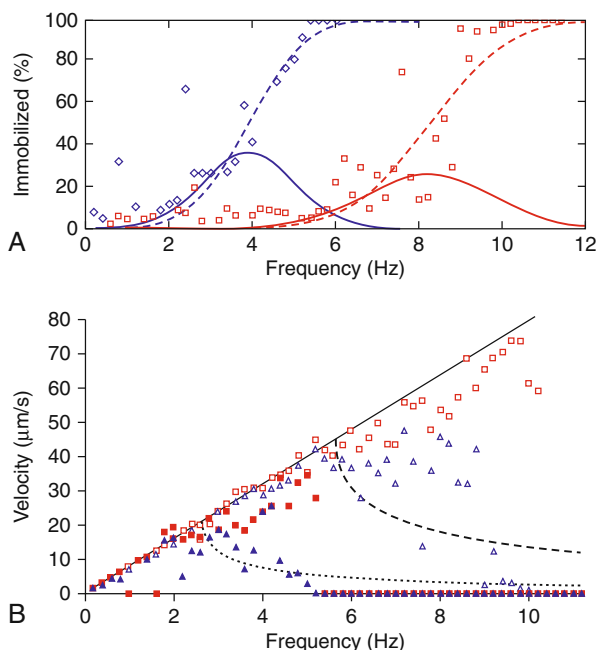


Fig. 19.4 (A) Percentage of immobile 1.0 μm (\diamond) and 2.7 μm particles (\square) is plotted as a function of the frequency of rotation of the external magnetic field. The cumulative distribution function (CDF) and probability distribution function (PDF) are presented as *dashed* and *solid* lines, respectively. In (B), the velocity of the 1.0 μm ($\blacktriangle, \blacklozenge$) and 2.7 μm particles (\triangle, \square) is presented as a function of the rotation frequency. The *squares* represent the mean velocity of the mobile particles, while the *triangles* represent the mean velocity of the entire population of particles. The *dashed* or *dotted* lines are the simulated velocity for the 2.7 μm and 1 μm particles, respectively, based on an appropriate choice for the critical frequency for each particle size. *Reproduced by permission of The Royal Society of Chemistry* [8]

structures which can be formed inside fluids. In general, the forces can be either attractive or repulsive depending upon the relative position and orientation of the particles [29]. As seen in Fig. 19.5, attractive forces exist between two identical particles when the position vector connecting the particle centers is parallel to the local field (i.e., opposite poles are in close proximity). Repulsive forces are present when this position vector is perpendicular to the local field (i.e., magnetic equators are in close proximity). This anisotropic behavior leads to the pole-to-pole chaining of similar particles that has been well characterized [52–54].

In computing forces between particles in the suspension, it is important to account for both the field and the field gradient of one particle on another. Assuming that these particles behave approximately as dipoles, the field of a particle, \vec{H}_p , can be determined from the classical dipole field equation [35]:

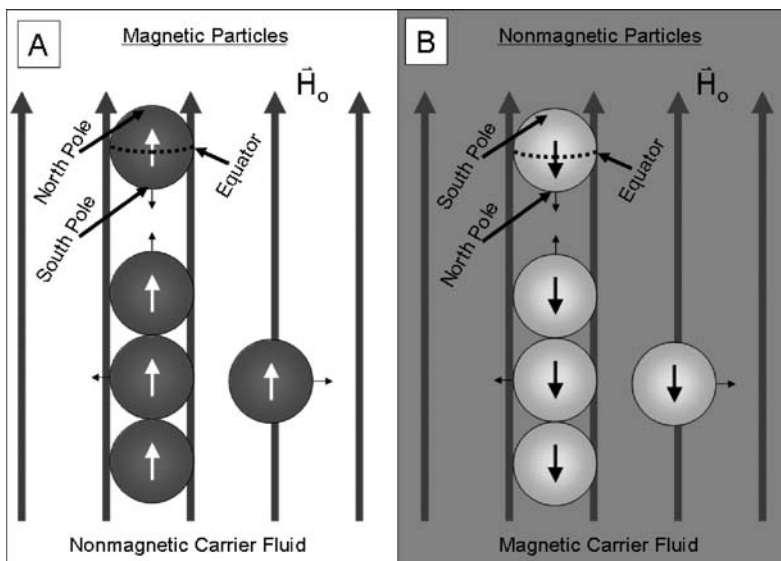


Fig. 19.5 (A) Magnetic particles suspended in a nonmagnetic carrier fluid form chains in local field, \vec{H}_0 . The particles' moments align parallel with the field. (B) Nonmagnetic particles suspended in a magnetic carrier fluid also form chains; however, the particle moments are aligned antiparallel with the field. In both cases, particles are attracted toward the magnetic poles of other particles and repelled from the magnetic equators, exemplified by the small force arrows

$$\vec{H}_p = \frac{3[V_p(\vec{M}_p - \vec{M}_f) \cdot \vec{r}] \cdot \vec{r}}{r^5} - \frac{V_p(\vec{M}_p - \vec{M}_f)}{r^3} \quad (19.11)$$

where \vec{r} is the distance between the point of observation and the particle location. It is important to note that the magnetization of the particle is a function of the local field, which includes the fields produced by neighboring particles. In a system with more than one particle, the field needs to be solved self-consistently [55].

In general, the formation of particle chains is a time-dependent process dominated by translational diffusion on the long length scale. For two particles or chains of particles to link, the groups need to diffuse through the suspension until their proximity substantially increases the magnetic attraction energy between them, at which point the particle trajectory becomes dominated by magnetic force. This type of chain growth is a random-walk, Smulochowski-type growth that has been investigated in the past [60, 61, 62]. Two particles will only be significantly attracted or repelled from one another if the change in potential energy experienced by the particle as it moves a distance of one particle diameter becomes significant relative to $k_B T$. At this point, the particles undergo a transition from Brownian-dominated motion to trajectory-dominated motion, and the chain formation process quickly occurs.

19.4.2 Magnetic and Nonmagnetic Mixed Assemblies in Ferrofluid

An interesting branch of these physical systems occurs when several different types of particles are mixed together, such as the mixture of magnetic particles, nonmagnetic particles, and ferrofluid. The magnetic particles will behave as positive dipoles if their magnetization is stronger than that of the ferrofluid, while the nonmagnetic particles still behave as negative dipoles. The net effect is that the magnetic and nonmagnetic particles will still attract one another; however, the magnetic and nonmagnetic particles will not align head to tail, but instead will align in an anti-ferromagnetic fashion.

In these systems, interesting structures have been observed to self-organize depending on the applied field strength, the bulk ferrofluid concentrations, and the sizes of the particles. For example, if commensurately sized magnetic and nonmagnetic particles are suspended within ferrofluid, they can form simple cubic rectangular arrays in an applied external field as seen in Fig. 19.6A,C.

In addition to these particle arrays, other self-assembled structures can be observed in mixed suspensions when the magnetic and nonmagnetic particles are of two different sizes. For example, if one of the particles is much larger than the other (e.g., tripling the size of the highly magnetic particles as seen in Fig. 19.6B), Saturn-like structures take form as the smaller particles are attracted only to the magnetic equator of the large particle, shown also in Fig. 19.6D,E [56].

19.4.3 Anisotropic Particle Alignment

In addition to translational forces, torques also can be applied to particles that have shape anisotropy. This effect can occur for either magnetic or nonmagnetic particles depending on the surrounding fluid magnetization. The energetics of particle alignment is schematically illustrated in Fig. 19.7, in which a magnetized particle develops magnetic poles on its surface which act to oppose the field \vec{H} within the particle. This field, known as the demagnetizing field, \vec{H}_D , contributes to the total magnetic field within the interior of the particle, \vec{H}_{int} , according to the following equation:

$$\vec{H}_{int} = \vec{H} - \vec{H}_D = \vec{H} - G(\vec{M}_p - \vec{M}_f) \quad (19.12)$$

Here the tensor G represents the demagnetizing factor and is based solely on the particle's aspect ratio and the direction of the external field. In general, demagnetizing factors are smaller when the longest particle axis (i.e., the easy axis) is aligned with the field.

Though many particles can be approximated as spherical, there exist many particle geometries that are better modeled as ellipsoids [57, 58], such as rod-like colloidal particles which can be represented very accurately as prolate spheroids when

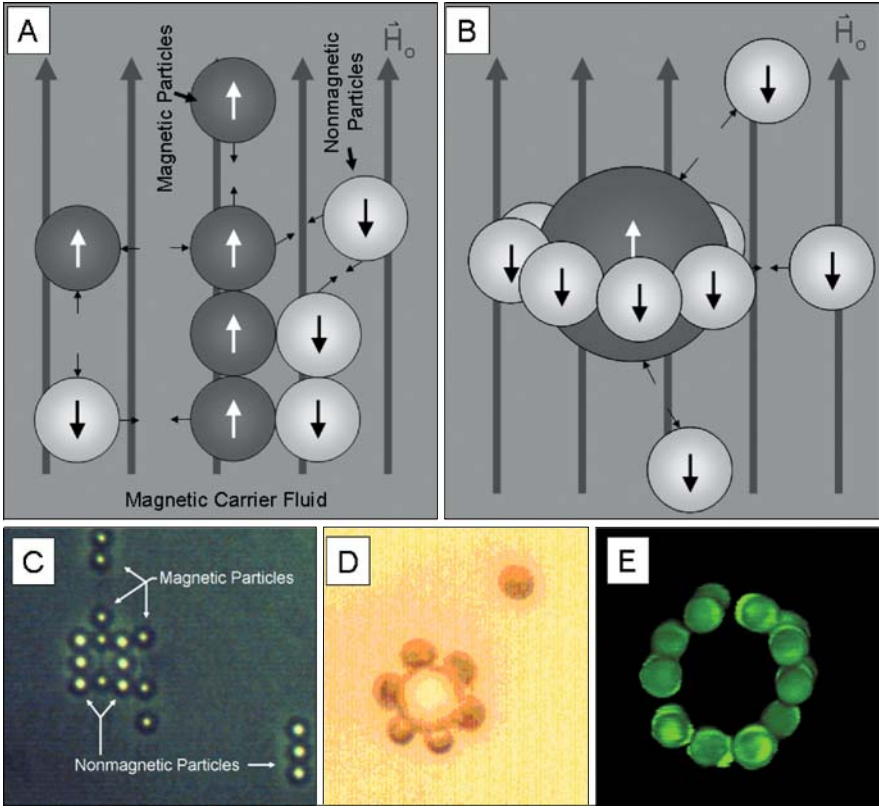


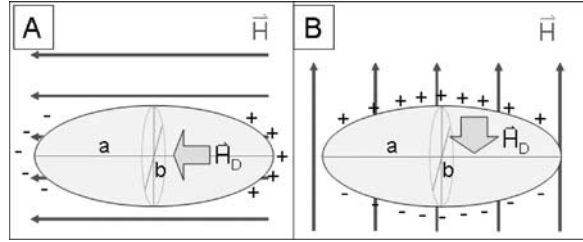
Fig. 19.6 (A) Equal-sized nonmagnetic and magnetic microparticles suspended in ferrofluid form array-like structures. (B) Enlarging one particle size leads to ring-like structures. Simplified directional forces are shown with small *arrows*. (C) Micrograph showing 3 μm magnetic and 3 μm nonmagnetic particles forming a simple cubic lattice in ferrofluid. (D) Micrograph of 1 μm magnetic particles forming a *ring* around a 3 μm nonmagnetic particle in ferrofluid. (E) Fluorescent micrograph of 1 μm nonmagnetic particles forming around a 3 μm magnetic particle (non-fluorescent) into a *ring* structure in ferrofluid

the aspect ratio is larger than 10. When the long axis of the prolate spheroid, labeled a in Fig. 19.7, is aligned parallel or perpendicular to \vec{H} , the respective demagnetizing factors of G_a and G_b are well established [67]:

$$G_a = \frac{(a/b)^2}{2} \int_0^\infty \frac{ds}{(s+a^2)^{3/2}(s+b^2)}, G_b = \frac{(a/b)^2}{2} \int_0^\infty \frac{ds}{(s+a^2)^{1/2}(s+b^2)^2} \tag{19.13}$$

As seen in Eq. (19.13), alignment away from the easy axis requires more energy to achieve due to substantial increase in demagnetizing fields. Because particles are more likely to be in lower energy states, the particle experiences a torque driving

Fig. 19.7 A magnetic ellipsoidal particle shown in a local field directed (A) parallel and (B) perpendicular to the easy axis, a . Magnetic poles on the particle surfaces create a demagnetizing field, \vec{H}_D , within the particle



its easy axis to point along the external field direction. The rotational energy of an ellipse aligned at an angle of θ from the magnetic field is well characterized and found to be [59, 60]:

$$U(\theta) = \frac{2\pi ab^2}{3} \frac{\mu_f (\mu_p - \mu_f)^2 (G_b - G_a) H^2 \sin^2(\theta)}{(\mu_f - (\mu_p - \mu_f) G_a) (\mu_f - (\mu_p - \mu_f) G_b)} \tag{19.14}$$

where μ_p and μ_f are the respective magnetic permeabilities of the particle and the fluid derived from the material susceptibility (e.g., $\mu_p = \mu_o (1 + \chi_p)$).

This rotational energy can be used to determine the alignment distribution within a population of prolate spheroids using a Boltzmann distribution function. For larger particles with strong fluid magnetization mismatches, the rod’s alignment is completely determined by the direction of the external field; however, smaller particles can experience larger orientational variation when the average alignment energy, $\langle U(\theta) \rangle$, is close to thermal fluctuation energy. The average energy of particle alignment energy is given by

$$\langle U(\theta) \rangle = \frac{\int_0^{2\pi} U(\theta) e^{-U(\theta)/k_B T} d\theta}{\int_0^{2\pi} e^{-U(\theta)/k_B T} d\theta} \tag{19.15}$$

In order to describe the orientation variation, nematic order parameters [62] can be used such as $S = \langle (3 \cos^2 \theta - 1) / 2 \rangle$ where S ranges from 0, for completely disordered suspensions of particles, to 1, for completely ordered suspensions of particles. For a suspension of magnetic or nonmagnetic elliptical particles within nonmagnetic or magnetic carrier fluid, respectively, typical order parameters, like those shown in Fig. 19.8, depend upon particle geometry, surrounding fields, and relative magnetizations. Such studies have been carried out for both nonmagnetic rods in ferrofluid [63], seen in Fig. 19.8, and magnetic particles in water [64].

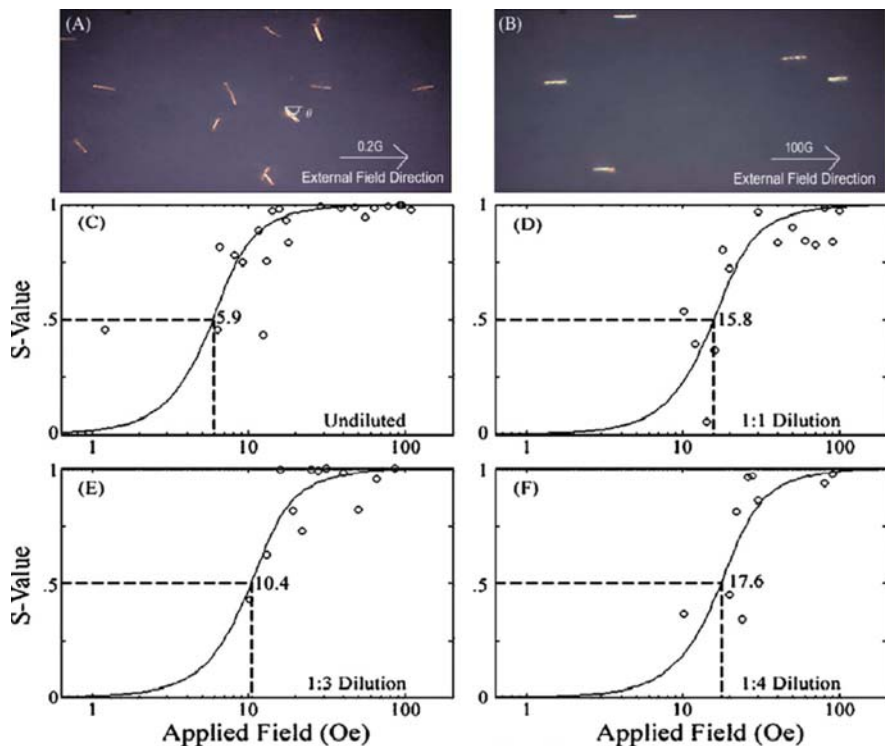


Fig. 19.8 Optical micrographs (A) and (B) demonstrate the orientation distribution of nonmagnetic nanorods in ferrofluid for external fields of (A) 0.2 G and (B) 100 G. Data in (C–F) show the effective orientation of nanorods at ferrofluid volume fractions of (C) 3.6%, (D) 1.8%, (E) 1.2%, and (F) 0.9%. The theoretical fitting curves from the nematic order parameter S are shown by the solid lines and demonstrate a nice fit of the experimental data points. Reused with permission from Chinchun Ooi, *Journal of Applied Physics*, 103, 07E910 (2008). Copyright 2008, American Institute of Physics [61]

19.5 Brownian-Dominated Manipulation of Particle Populations

19.5.1 Modeling Thermal Diffusion

When the nanoparticle is reduced to a critical size, its motion becomes dominated by Brownian diffusion regardless of the applied field, and the role of thermal fluctuations in modeling the distribution within nanoparticle suspensions can become very important. Moreover, at these length scales, the thermal energy of the particles, $k_B T$, may no longer be diminutive relative to the particle's magnetization energy, $M_s V H$, even in strong magnetic fields. Thus, the role of thermal fluctuations in several aspects will need to be incorporated in order to attain representative models. The models will no longer follow the individual trajectories of nanoparticles but instead will be concerned with the average particle flux in the statistical sense. The overall

flux of the local particle concentrations, \vec{J}_{net} , can be modeled through the sum of the thermally driven diffusion flux, $\vec{J}_{diffusion}$, and the deterministically forced drift flux, \vec{J}_{drift} . The diffusion flux is proportional to the local diffusion coefficient, D , and the local variation of the particle concentration, C , as $\vec{J}_{diffusion} = -D\nabla C$. The drift flux is also based on the velocity of the particle, \vec{v}_p , due to migration forces as $\vec{J}_{drift} = \vec{v}_p C$. The local net particle flux is time dependent and can be written in terms of the continuity equation: $-\nabla \cdot \vec{J}_{net} = \partial C / \partial t$. The encompassing characterizing equation for the local net particle flux, known as Fick's Law [65], can be written as follows:

$$\partial C / \partial t = -\nabla \cdot \vec{J}_{net} = -\nabla \cdot (\vec{J}_{drift} - \vec{J}_{diffusion}) = -\nabla \cdot (\vec{v}_p C - D\nabla C) \quad (19.16)$$

There arises a special case for this equation where the drift and the diffusion fluxes exactly balance. This can be viewed as a quasi-equilibrium state where, although the individual particles have a nonzero velocity, the average particle population densities are static. In this case, where $\partial C / \partial t = 0$, concentration distributions can be obtained by solving the equation $\vec{v}_p C = D\nabla C$ if the local particle velocity and the diffusion coefficient are known or can be calculated.

In a viscous medium where inertial effects are unimportant, there is a direct relationship between the magnetic force \vec{F}_p and the particle's velocity according to $\vec{v}_p = \eta \vec{F}_p$, where η is the hydrodynamic mobility of the particle. Inserting this relationship into Eq. (19.16) under steady-state conditions yields

$$\frac{\nabla C}{C} = \frac{\eta}{D} \vec{F}_p \quad (19.17)$$

The Einstein relation, $D = \eta k_B T$, presents a convenient simplification at this point. This relation assumes that the diffusion coefficient and particle mobility are independent of local particle concentration which is a good assumption in dilute suspensions [41]. However, in the case of very high local particle concentrations, this relation may not be accurate and a concentration-dependent diffusion coefficient is needed.

Assuming the force is given by Eqs. (19.2), (19.17) can be rewritten as

$$\frac{\nabla C}{C} = \frac{\mu_o}{k_B T} V \left[\left(\vec{M}_p - \langle \vec{M}_f \rangle \right) \cdot \nabla \right] \vec{H} \quad (19.18)$$

Here, V represents the volume of the effective ferrofluid particle size, and $k_B T$ is taken as a constant assuming isothermal equilibrium conditions. This equation is general as it allows for the local concentration to be obtained for both magnetic and nonmagnetic particles based upon the local magnetic field and the particle and fluid magnetizations. When the Langevin saturation model is combined with Eq. (19.18), the following differential equation is obtained:

$$\frac{\nabla C}{C} = \frac{\mu_o}{k_B T} V \left[\left(\vec{M}_p - M_s C_m L(\xi) \hat{H} \right) \cdot \nabla \right] \vec{H} \quad (19.19)$$

This equation can be used either to model the local concentration of the ferrofluid particles, in which case the parameters become $C = C_m$ and $\vec{M}_{p,m} = M_s L(\xi) \hat{H}$, or to model the local concentration of nonmagnetic particles within the ferrofluid, in which case the parameters become $C = C_n$ and $\vec{M}_{p,n} = 0$.

19.5.2 Magnetic Particle Concentration

Initially, we restrict our discussion of Eq. (19.19) to model the local concentration of the magnetic particles that comprise the ferrofluid. This is the logical starting point as the system becomes even more complicated when nonmagnetic particles are introduced. For a suspension of magnetic particles, Eq. (19.19) becomes

$$\frac{\nabla C_m}{C_m (1 - C_m)} = L(\xi) \nabla \xi \quad (19.20)$$

This represents a first-order differential equation that can only be analytically integrated when ξ is independent of C_m . However, some caution must be taken when using this model. In the present representation of Eq. (19.20), the magnetic energy is assumed to be independent of the local particle concentration. When the volume fraction of magnetic particles is large ($>5\%$ V.F.), particles can be shielded by their neighbors, effectively lowering the local magnetic field that determines $\xi(\vec{H})$. In order to incorporate this shielding phenomenon, the local magnetic field must be solved at the same time as solving for the local particle concentration (i.e., $\vec{H}(C_m)$). By solving this continuum model self-consistently, the fluid magnetization is more accurate in both the high-field and the high-concentration regimes. However, this self-consistent solution prevents the derivation of analytic models that are useful for first-order approximations or for systems with relatively low particle concentration. In relatively low concentrations, minor errors may be acceptable, in which case an analytical expression can be obtained for particle concentration. Equation (19.20) can be directly integrated to yield

$$\frac{C_m}{(1 - C_m)} = A \frac{\sinh(\xi)}{\xi} \quad (19.21)$$

where $A = C_m \xi / [(1 - C_m) \sinh(\xi)]$ is an integration constant that can be solved through forcing the resultant equation to satisfy bulk conditions in a gradient-free regions. Away from field gradients, the local particle concentrations must equal bulk particle concentrations, Φ_m , and the local field will be equal to the magnetic field external to any local magnetic sources that has an energy ratio of ξ_o . Substitution of the boundary conditions leads to the integration constant,

$A = \Phi_m \xi_o / [(1 - \Phi_m) \sinh(\xi_o)]$. By inserting the integration constant back into Eq. (19.21), the local concentration of the magnetic particles within ferrofluid can be attained:

$$C_m = \left(1 + \frac{(1 - \Phi_m) \sinh(\xi_o) \xi}{\Phi_m \sinh(\xi) \xi_o} \right)^{-1} \quad (19.22)$$

Equation (19.22) is very useful as it can predict the local particle concentration as a function solely of the local energy ratio, ξ . In addition, Eq. (19.22) exhibits the appropriate asymptotic behavior; at very large local fields, ($\xi \gg \xi_o$), $C_m \rightarrow 1$, and at very small local fields, ($\xi \ll \xi_o$), $C_m \rightarrow 0$. An experimental image of a typical ferrofluid concentrating near high-gradient magnetic sources is presented in Fig. 19.9A. Here, the ferrofluid particles concentrate very densely between rectangular islands, where the fields created by the islands add to a transverse external field.

Experimental work has verified the accuracy of this expression in regions of strong field and relatively low particle concentrations through the use of optical absorption measurements [10]. Attenuation of the intensity of light through a distance r of ferrofluid follows a well-defined Beer–Lambert relationship of $I = I_o e^{-\alpha r}$. Here α is a material-dependent absorption coefficient that needs to be experimentally determined independently for a ferrofluid. For example, the well-characterized ferrofluid EMG 705 from Ferrotec (Nashua, NH) shown in Fig. 19.9A is found to exhibit an adsorption coefficient of $\alpha = K (C_m)^\beta / (2L)$, where K and β are proportionality constants and $2L$ is the total path length the light travels (twice the fluid height for a reflected light microscopy setup). For a fluid height of 3 μm , a calibration curve was created, shown in Fig. 19.9B, that relates the bulk particle concentration to collected light intensity. For proper characterization of this calibration data, the proportionality constants were found to be $K = 9.24$ and $\beta = 0.79$.

With this calibration relationship established, a theoretical light intensity can be calculated for suspensions of ferrofluid near micromagnets. To determine these intensities, the Beer–Lambert relationship can be integrated across the fluid height to account for variation in particle concentration with height above the micromagnets as

$$I(x, y) = 2 \int_0^L e^{-KzC_m^\beta/L} dz \quad (19.23)$$

Equation (19.23) allows for a theoretical relationship between local field energies and light intensities to be established and correlated to the local concentration profile of ferrofluid. For different bulk particle concentrations, this relationship produces different plots as shown in Fig. 19.9C. Using photo analysis software, the relative light intensities of experimentally collected micrographs, such as the one in Fig. 19.9A, can be directly compared to the theoretical plots as presented with dotted lines in Fig. 19.9C. For these experiments, the areas directly between two islands were sampled for intensity data for two reasons. First, the particle concentrations in

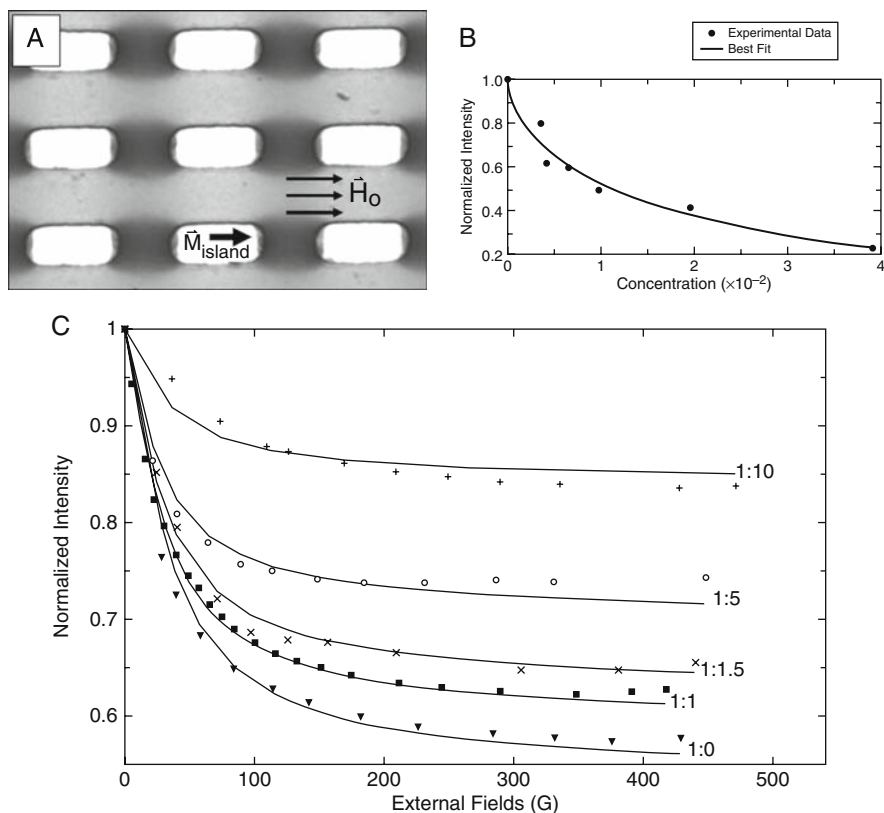


Fig. 19.9 (A) Experimental micrograph shows rectangular cobalt islands that are $8 \mu\text{m}$ by $4 \mu\text{m}$. Magnetic ferrofluid particles concentrate between the islands in the field maxima. (B) A calibration curve is shown comparing bulk concentration versus bulk light intensity. (C) Plots of local concentration of magnetic particles versus local field for different dilutions of ferrofluid. The local concentration can be described fairly accurately using Eq. (19.22) with an effective nanoparticle diameter of $\sim 24 \text{ nm}$. Reused with permission from Randall M. Erb, *Journal of Applied Physics*, 103, 063916 (2008). Copyright 2008, American Institute of Physics [10]

these areas are within the low-concentration regime ($< 10\%$ V.F.), which is necessary for the validity of Eq. (19.22). Second, the fields produced by cobalt thin-film islands can be well predicted at large distances away from the islands poles (i.e., distances on the order of the width of an island).

Our experimental results indicated that the ferrofluid is best characterized by an average aggregate size, which is much larger than the individual ferrofluid particles observed within the suspension. The underlying reason for this effect can be explained from aggregation phenomenon occurring in colloidal physics. For example, other forces in colloidal suspensions exist including steric, electrostatic, Van der Waals, and depletion forces, some of which are attractive and others repulsive. In general, all colloidal suspensions are thermodynamically unstable due to the deep

attractive potential energy minimum when two particles are touching; however due to the presence of a repulsive energy barrier, the time scales over which particles aggregate can be sufficiently long to consider them stable. For certain sized colloids, the attractive Van der Waals forces, which scale with the particle radius, may be stronger than the repulsive electrostatic forces, which scale with the total charge on the particle. The net result is that aggregation will be present; however, the aggregation has been shown to be self-limiting based on generic scaling relationships between these attractive and repulsive interactions [66]. Specifically, it has been shown that when the repulsive energy barrier between neighboring particles exceeds $15k_B T$, the suspension is conventionally considered stable. If the energy barrier is smaller, then the particles within the suspension will aggregate until this constraint is met. This self-limiting aggregation is common in particle suspensions, and the average particle size is often well larger than an individual particle at conception [67–70]. These large average aggregate sizes must be included to form a realistic model for the particle suspension since the larger magnetic volumes of the aggregates play a major role in the force upon a particle and, ultimately, its velocity. For this reason, it was not surprising that the ferrofluid particles in our experiments were behaving as small aggregates.

19.5.3 Nonmagnetic Particle Concentrations

Once the magnetic nanoparticle concentration can be determined, it is possible to describe the local particle concentration of nonmagnetic particles, C_n , submerged within a ferrofluid. In this situation, the nonmagnetic particles have negligible magnetization ($\vec{M}_{p,n} = 0$), and Eq. (19.19) becomes

$$\frac{\nabla C_n}{C_n} = -\gamma C_m L(\xi) \nabla \xi \quad (19.24)$$

where $\gamma = V_n/V_m$ represents a nondimensional size ratio between the ferrofluid and nonmagnetic particles. Equation (19.24) indicates that the concentration of nonmagnetic particles depends upon the local ferrofluid concentration, which considerably complicates the general analysis. For scenarios where the ferrofluid is in the high-concentration regime, C_m , a self-consistent approach should be used to solve Eq. (19.20). If the ferrofluid concentration is reasonably low, then Eq. (19.22) can be inserted into Eq. (19.24) and an analytic expression can be obtained. Considering the low-concentration regime, Eq. (19.24) can be integrated as

$$C_n = A^{-1} \left[2 \frac{\sinh(\xi)}{\xi} + 2 \left(\frac{1 - \Phi_m \sinh(\xi_o)}{\Phi_m \xi_o} \right) \right]^{-\gamma} \quad (19.25)$$

where the integration constant, A , can again be arrived at by satisfying bulk conditions within gradient-free regions. In these regions, the local nonmagnetic particle concentration must equal the nonmagnetic bulk concentration, Φ_n , and the local

magnetic energy will be equal to the bulk energy ratio of ξ_o . Satisfying these requirements determines the value of the integration constant which can be incorporated into Eq. (19.25) to yield

$$C_n = \Phi_n \left[1 + \Phi_m \left(\frac{\sinh(\xi)}{\sinh(\xi_o)} \frac{\xi_o}{\xi} - 1 \right) \right]^{-\gamma} \tag{19.26}$$

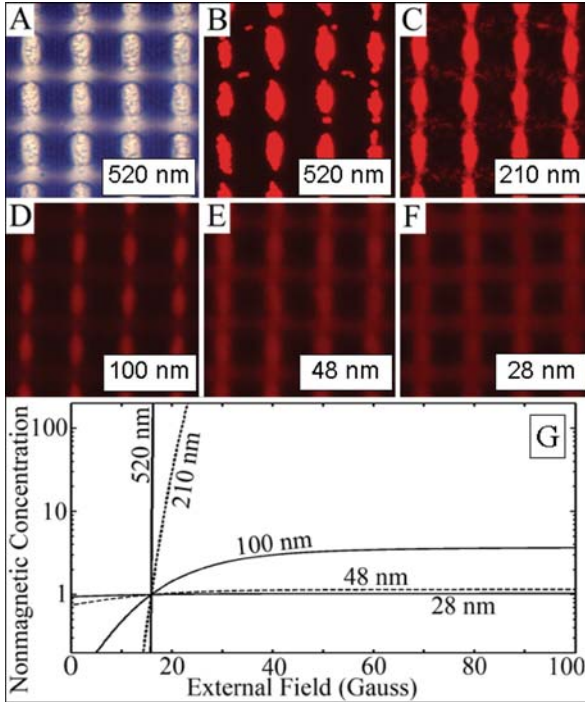


Fig. 19.10 (A) Bright field and (B–F) fluorescent images of 5 μm circular cobalt ferromagnetic islands magnetized in an external field directed rightward. On top of the islands, nonmagnetic particles in ferrofluid concentrate to different extents depending on particle size. (G) Plots of local concentration of nonmagnetic particles versus external field for different sizes of nanoparticles with bulk volume fractions of particles and ferrofluids as 1% and 3.6%, respectively. Below ~ 15 Gauss, the external field is too weak to create field minima on top of the islands, and the nonmagnetic particles are forced away. *Reused with permission from Randall M. Erb, Journal of Applied Physics, 103, 07A312 (2008). Copyright 2008, American Institute of Physics [28]*

In regions of very high local field, where the ferrofluid particles will densely concentrate, Eq. (19.26) shows the nonmagnetic particle concentration to approach 0. This expression, unlike Eq. (19.22), has no inherent saturation since the nonmagnetic concentration will breach the non-physical close-packing threshold with large enough local fields. To resolve this, an artificial restriction on the geometric packing factor can be placed upon Eq. (19.26) that limits the possible values

of the concentration strictly to those that are physical (e.g., $C_n \leq 1$). The main benefit of Eq. (19.26) is that it conveniently predicts the local concentration of nonmagnetic particles based only upon local energy ratios, size ratios, and bulk concentrations.

To test the validity of Eq. (19.26), nonmagnetic fluorescent polystyrene particles of various sizes were mixed with 705 EMG ferrofluid and concentrated on top of cobalt islands, shown in Fig. 19.10A–F [28]. For these experiments, the fluid height was held at 3 μm , and the bulk volume fraction of ferrofluid and nonmagnetic particles were 3.6% and 1.0%, respectively. Nonmagnetic particle sizes of 210 and 520 nm are seen to close-pack on top of the magnetic islands. Conversely, the 24 and 48 nm particles do not seem to concentrate substantially on the islands, while the 100 nm particles somewhat concentrate. In comparison with these experimental studies, the behavior of Eq. (19.26) for these experimental bulk conditions is plotted in Fig. 19.10G across different field strengths and particle sizes. Comparison between these plots and the experimental fluorescent micrographs confirms a qualitative agreement between theoretical predictions and experimental results, and moreover it indicates that continuum equations are still reasonably accurate even when the nonmagnetic nanoparticles are only 2–3 times larger than the magnetic nanoparticles in the fluid.

19.5.4 Applications of Concentration Gradients

The concentration gradients that arise in various ferrofluid mixtures are complex phenomena that lend themselves to certain unique applications. The particles within a magnetic particle suspension can be strongly concentrated within certain regions of HGMS systems, and in some cases can reach close-packing, which implies a localized phase transformation has occurred in the fluid. Regions of the substrate where the particles become close-packed will experience substantial changes in the local viscosity and rheological properties. Furthermore, these regions become effectively inaccessible (i.e., masked) from the surrounding suspension. For example, these close-packed regions can be used as a UV photomask to block light from interacting with the underlying surface [71–72].

In addition to blocking electromagnetic waves, these close-packed particles can possibly block certain chemical hybridization reactions from taking place. Such applications are enhanced since in the regions of high magnetic concentration there are very low concentrations of nonmagnetic particles as per Eq. (19.26). For this reason, magnetically programming the chemisorption or physisorption of nonmagnetic particles onto surfaces becomes physically plausible as demonstrated in Fig. 19.11. This technique can be used for applications including cell manipulation, concentration of fluorescent labels onto biosensors, and even production of protein arrays. However, due to the recent development of this niche of colloidal physics, there remain many applications yet to be conceived.

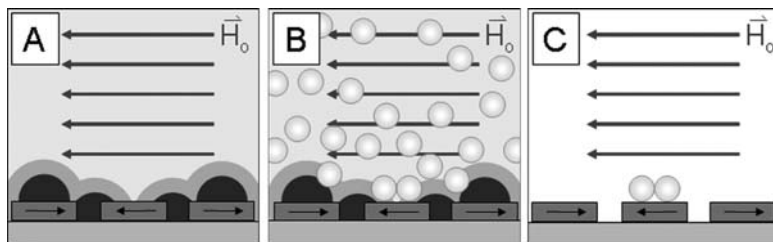


Fig. 19.11 Example setup of magnetically controlled adsorption of nonmagnetic particles to the surface. In **(A)**, ferrofluid is concentrated in regions to be blocked. In **(B)**, nonmagnetic particles are introduced into solution and allowed to diffuse throughout suspension, avoiding areas of high magnetic particle concentration. In **(C)**, suspension is rinsed or diluted and adsorbed particles remain

19.6 Conclusions and Outlook

Here we reviewed the magnetic manipulation of particles within suspensions. Compared with other reviews that focused on high-gradient magnetic separation systems, including by one of the authors, this chapter has instead focused on the magnetic manipulation of mixed suspensions of magnetic and nonmagnetic particles. In this chapter, we developed a theoretical basis for determining the effect of Brownian motion within a system, through determining the magnitude of the magnetic forces present. We first detailed several deterministic systems that are minimally influenced by Brownian motion, in which we described recent theoretical and experimental work on surface-based assembly and substrate-based transport of colloidal particles. Due to the programmability of these systems, they have potential in self-assembled fabrication techniques and lab-on-a-chip platforms. We then turned our attention to particle systems that can be influenced, but are not dominated, by Brownian motion. Several types of self-organizing structures we presented included particle arrays, particle rings, and chain growth. The use of multiple different colloidal components may lead to more complex assemblies than those presented here; thus, this field appears to be very promising for future discoveries. This discussion was followed by the analysis of Brownian-dominated systems, which despite the inherent randomness, can still allow for controllable manipulation of groups of colloidal particles. The theoretical predictions developed in this section based on ensemble modeling techniques for determining local particle concentrations were shown to agree reasonably well with experimental results. However, these models are limited to the low particle concentration regime, and future numerical work is needed to determine the degree of inaccuracy when these models are applied to regions of high particle concentrations.

References

1. Grier, D.G.: A revolution in optical manipulation. *Nature* **424** (6950), 810–816 (2003)
2. Ashkin, A., Dziedzic, J. M., Yamane, T.: Optical trapping and manipulation of single cells using infrared-laserbeams. *Nature* **330** (6150), 769–771 (1987)
3. Huang, Y., Ewalt, K. L., Tirado, M., Haigis, T. R., Forster, A., Ackley, D., Heller, M. J., O'Connell, J. P., Krihak, M.: Electric manipulation of bioparticles and macromolecules on microfabricated electrodes. *Analytical Chemistry* **73** (7), 1549–1559 (2001)
4. Pethig, R.: Dielectrophoresis: Using inhomogeneous AC electrical fields to separate and manipulate cells. *Critical Reviews in Biotechnology* **16** (4), 331–348 (1996)
5. Helseth, L. E., Fischer, T. M., Johansen, T. H.: Domain wall tip for manipulation of magnetic particles. *Physical Review Letters* **91** (20), 208302 (2003)
6. Yellen, B. B., Hovorka, O., Friedman, G.: Arranging matter by magnetic nanoparticle assemblers. *Proceedings of the National Academy of Sciences* **102** (25), 8860–8864 (2005)
7. Yellen, B. B., Erb, R. M., Halverson, D. S., Hovorka, O., Friedman, G.: Arraying nonmagnetic colloids by magnetic nanoparticle assemblers. *IEEE Transactions on Magnetics* **42** (10), 3548–3553 (2006)
8. Yellen, B. B., Erb, R. M., Son, H. S., Hewlin Jr., R., Shang, H., Lee, G. U.: Traveling wave magnetophoresis for high resolution chip based separations. *Lab on a Chip* **7**, 1681–1688 (2007)
9. Gerber, R., Takayasu, M., Friedlaender, F. J.: Generalization of HGMS theory – the capture of ultrafine particles. *IEEE Transactions on Magnetics* **19** (5), 2115–2117 (1983)
10. Erb, R. M., Sebba, D. S., Lazarides, A. A., Yellen, B. B.: Magnetic field induced concentration gradients in magnetic nanoparticle suspensions: Theory and Experiment. *Journal of Applied Physics*. **103** (6), 063916–5 (2008)
11. Adair, R. K.: Constraints on Biological Effects of Weak Extremely-Low-Frequency Electromagnetic Fields. *Physical Review A* **43** (2), 1039–1048 (1991)
12. Grahl, T., Markl, H.: Killing of microorganisms by pulsed electric fields. *Applied Microbiology and Biotechnology* **45** (1–2), 148–157 (1996)
13. Peterman, E. J. G., Gittes, F., Schmidt, C. F.: “Laser-induced heating in optical traps” *Biophysical Journal* **84** (2), 1308–1316 (2003)
14. Friedman, G., Yellen, B.: Magnetic separation, manipulation and assembly of solid phase in fluids. *Current Opinion in Colloid and Interface Science* **10** (3–4), 158–166 (2005)
15. Ito, A., Shinkai, M., Honda, H., Kobayashi, T.: Medical application of functionalized magnetic nanoparticles. *Journal of Bioscience and Bioengineering* **100** (1), 1–11 (2005)
16. Gijs, M. A. M.: Magnetic bead handling on-chip: new opportunities for analytical applications. *Microfluidics and Nanofluidics* **1** (1), 22–40 (2004)
17. Gillies, G. T., Ritter, R. C., Broaddus, W. C., Grady, M. S., Howard, M. A., McNeil, R. G.: Magnetic manipulation instrumentation for medical physics research. *Review of Scientific Instruments* **65** (3), 533–562 (1994)
18. Xia, N., Hunt, T. P., Mayers, B. T., Alsborg, E., Whitesides, G. M., Westervelt, R. M., Ingber, D. E.: Combined microfluidic-micromagnetic separation of living cells in continuous flow. *Biomedical Microdevices* **8** (4), 299–308 (2006)
19. Hancock, J. P., Kemshead, J. T.: A rapid and highly selective approach to cell separations using an immunomagnetic colloid. *Journal of Immunological Methods* **164** (1), 51–60 (1993)
20. Heermann, K. H., Hagos, Y., Thomssen, R.: Liquid-phase hybridization and capture of Hepatitis-B virus-DNA with magnetic beads and fluorescence detection of PCR product. *Journal of Virological Methods* **50** (1–3), 43–57 (1994)
21. Pipper, J., Inoue, M., Ng, L. F. P., Neuzil, P., Zhang, Y., Novak, L.: Catching bird flu in a droplet. *Nature Medicine* **13** (10), 1259–1263 (2007)
22. Kim, S. K., Devine, L., Angevine, M., DeMars, R., Kavathas, P. B.: Direct detection and magnetic isolation of Chlamydia trachomatis major outer membrane protein-specific CD8(+) CTLs with HLA class I tetramers. *Journal of Immunology* **165** (12), 7285–7292 (2000)

23. De Palma, R., Reekmans, G., Liu, C. X., Wirix-Speetjens, R., Laureyn, W., Nilsson, O., Lagae, L.: Magnetic bead sensing platform for the detection of proteins. *Analytical Chemistry* **79** (22), 8669–8677 (2007)
24. Vatta, L. L., Sanderson, R. D., Koch, K. R.: Magnetic nanoparticles: Properties and potential applications. *Pure and Applied Chemistry* **78** (9), 1793–1801 (2006)
25. Okuno, M., Hamaguchi, H. O., Hayashi, S.: Magnetic manipulation of materials in a magnetic ionic liquid. *Applied Physics Letters* **89** (13), 132506 (2006)
26. Halverson, D., Kalghatgi, S., Yellen, B., Friedman, G.: Manipulation of nonmagnetic nanobeads in dilute ferrofluid. *Journal of Applied Physics* **99** (8), 08P504 (2006)
27. Erb, R. M., Yellen, B. B.: Model of detecting nonmagnetic cavities in ferrofluid for biological sensing applications. *IEEE Transactions on Magnetics* **42** (10), 3554–3556 (2006)
28. Erb, R. M., Yellen, B. B.: Concentration gradients in mixed magnetic and nonmagnetic colloidal suspensions. *Journal of Applied Physics* **103** : 07A312–3 (2008)
29. Jones, T. B., *Electromechanics of Particles*. Cambridge University Press, New York (1995)
30. Huang, Y., Pethig, R.: Electrode design for negative dielectrophoresis. *Measurement Science and Technology* **2** (12), 1142–1146 (1991)
31. Shkel, Y. M., Klingenberg, D. J.: Magnetorheology and magnetostriction of isolated chains of nonlinear magnetizable spheres. *Journal of Rheology* **45** (2), 351–368 (2001)
32. Ivanov, A. O., Wang, Z. W., Holm, C.: Applying the chain formation model to magnetic properties of aggregated ferrofluids. *Physical Review E* **69** (3), 031206 (2004)
33. Philipse, A. P., Maas, D.: Magnetic colloids from magnetotactic bacteria: Chain formation and colloidal stability. *Langmuir* **18** (25), 9977–9984 (2002)
34. Einstein, A.: The theory of the Brownian Motion. *Annalen Der Physik* **19** (2), 371–381 (1906)
35. Boal, A. K., Frankamp, B. L., Uzun, O., Tuominen, M. T., Rotello, V. M.: Modulation of spacing and magnetic properties of iron oxide nanoparticles through polymer-mediated ‘bricks and mortar’ self-assembly. *Chemistry of Materials* **16** (7), 3252–3256 (2004)
36. Lim, J. K., Tilton, R. D., Eggeman, A., Majetich, S. A.: Design and synthesis of plasmonic magnetic nanoparticles. *Journal of Magnetism and Magnetic Materials* **311** (1), 78–83 (2007)
37. Sun, S., Murray, C. B., Weller, D., Folks, L., Moser, A.: Monodisperse FePt Nanoparticles and Ferromagnetic FePt Nanocrystal Superlattices. *Science* **287** (5460), 1989 (2000)
38. Odenbach, S., Liu, M.: Invalidation of the Kelvin force in ferrofluids. *Physical Review Letters* **86** (2), 328–331 (2001)
39. Bowen, W. R., Liang, Y., Williams, P. M.: Gradient diffusion coefficients – theory and experiment. *Chemical Engineering Science* **55** , 2359–2377 (2000)
40. Israelachvili, J. N., *Intermolecular and Surface Forces*. Academic Press, New York (1985)
41. Kelland, D. R., Hiresaki, Y., Friedlaender, F. J., Takayasu, M.: Diamagnetic particle capture and mineral separation. *IEEE Transactions Magnetics* **17** , 2813–2815 (1981)
42. Ferreira, H. A., Graham, D. L., Freitas, P. P., Cabral, J. M. S.: Biodetection using magnetically labeled biomolecules and arrays of spin valve sensors (invited). *Journal of Applied Physics* **93** (10), 7281–7286 (2003)
43. Baselt, D. R., Lee, G. U., Natesan, M., Metzger, S. W., Sheehan, P. E., Colton, R. J.: A biosensor based on magnetoresistance technology. *Biosens Bioelectron* **13** , 731–739 (1998)
44. Ivanov, A. O., Kantorovich, S. S., Reznikov, E. N., Holm, C., Pshenichnikov, A. F., Lebedev, A. V., Chremos, A., Camp, P. J.: Magnetic properties of polydisperse ferrofluids: A critical comparison between experiment, theory, and computer simulation. *Physical Review E* **75** (6), 061405 (2007)
45. Bradbury, A., Menear, S., Chantrell, R. W.: A Monte-Carlo calculation of the magnetic-properties of a ferrofluid containing interacting polydispersed particles. *Journal of Magnetism and Magnetic Materials* **54** (7), 745–746 (1986)
46. Brown, W. F.: Thermal fluctuations of a single-domain particle. *Physical Review* **130** (5), 1677–1686 (1963)
47. Madou, M. J., *Fundamentals of Microfabrication*. CRC Press, New York (2002)
48. Morse, P. M., Feshbach, H., *Methods of theoretical physics*. McGraw-Hill, New York (1953)

49. McNaughton, B. H., Kehbein, K. A., Anker, J. N., Kopelman, R.: Sudden breakdown in linear response of a rotationally driven magnetic microparticle and application to physical and chemical microsensing. *The Journal of Physical Chemistry*. **110** , 18958–18964 (2006)
50. Bonin, K., Kourmanov, B., Walker, T. G.: Light torque nanocontrol, nanomotors and nanorockers. *Optics Express*. **10** , 984–989 (2002)
51. Reichhardt, C., Nori, F.: Phase locking, devil's staircases, Farey trees, and Arnold tongues in driven vortex lattices with periodic pinning. *Physical Review Letters*. **82** , 414 (1999)
52. Fermigier, M., Gast, A.: Structure evolution in a paramagnetic latex suspension. *Journal of Colloid and Interface Science*. **154** , 522–539 (1992)
53. Promislow, J. H. E., Gast, A. P., Fermigier, M.: Aggregation kinetics of paramagnetic colloidal particles. *The Journal of Physical Chemistry*. **102** , 5492–5498 (1995)
54. Hagenbuchle, M., Liu, J.: Chain formation and chain dynamics in a dilute magnetorheological fluid. *Applied Optics* **36** (30), 7664–7671 (1997)
55. Yellen, B., Friedman, G., Feinerman, A.: Analysis of interactions for magnetic particles assembling on magnetic templates. *Journal of Applied Physics* **91** (10), 8552–8554 (2002)
56. Son, H.S., R.M. Erb, B. Samanta, V.M. Rotello, and B.B. Yellen, *Magnetically actuated assembly of anisotropic micro- and nano-structures*. Nature, 2008 (in submission): 1–4.
57. Camp, P. J., Allen, M. P., Hard ellipsoid rod-plate mixtures: Onsager theory and computer simulations. *Physica A* **229** (3–4), 410–427 (1996)
58. San Martin, S. M., Sebastian, J. L., Sancho, M., Miranda, J. M.: A study of the electric field distribution in erythrocyte and rod shape cells from direct RF exposure. *Physics in Medicine and Biology*. **48** (11), 1649–1659 (2003)
59. Kao, K.C.: Some electromechanical effects on dielectrics. *British Journal of Applied Physics*. **12** , 629–632 (1961)
60. Stratton, J.A., *Electromagnetic Theory*. McGraw-Hill, New York (1941)
61. Ooi, C., R.M. Erb, and B.B. Yellen, On the controllability of nanorod alignment in magnetic fluids. *Journal of Applied Physics*. 2008. **103** (7): 07E910-3.
62. Crawford, G. P., OndrisCrawford, R. J., Doane, J. W.: Systematic study of orientational wetting and anchoring at a liquid-crystal-surfactant interface. *Physical Review E*. **53** (4), 3647–3661 (1996)
63. Ooi, C., R.M. Erb, and B.B. Yellen, On the controllability of nanorod alignment in magnetic fluids. *Journal of Applied Physics*. 2008. **103** (7): 07E910-3.
64. Tanase, M., Felton, E. J., Gray, D. S., Hultgren, A., Chen, C. S., Reich, D. H., Assembly of multicellular constructs and microarrays of cells using magnetic nanowires. *Lab on a Chip*. **5** (6), 598–605 (2005)
65. Truskey, G. A., Yuan, F., Katz, D. F., *Transport Phenomena in Biological Systems*. Pearson Education, Inc., Upper Saddle River (2004)
66. Meyer, M., Le Ru, E. C., Etchegoin, P. G.: Self-limiting aggregation leads to long-lived metastable clusters in colloidal solutions. *The Journal of Physical Chemistry B*. **110** (12), 6040–6047 (2006)
67. Ivanov, A. O., Kuznetsova, O. B.: Magnetic properties of dense ferrofluids: An influence of interparticle correlations. *Physical Review E*. **64** (4), 041405–12 (2001)
68. da Silva, M. F., Neto, A. M. F.: Optical- and x-ray-scattering studies of ionic ferrofluids of MnFe₂O₄, γ-Fe₂O₃, and CoFe₂O₄. *Physical Review E*. **48** (6), 4483–4491 (1993)
69. Weber, J. E., Goni, A. R., Pusiol, D. J., Thomsen, C.: Raman spectroscopy on surfactated ferrofluids in a magnetic field. *Physical Review E*. **66** (2), 021407-06 (2002)
70. Kruse, T., Krauthäuser, H. G., Spanoudaki, A., Pelster, R.: Agglomeration and chain formation in ferrofluids: Two-dimensional x-ray scattering. *Physical Review B*. **67** (9), 094206-10 (2003)
71. Yellen, B. B., Fridman, G., Friedman, G.: Ferrofluid lithography. *Nanotechnology* **15** (10), S562–S565 (2004)
72. Yellen, B. B., Friedman, G., Barbee, K. A.: Programmable self-aligning ferrofluid masks for lithographic applications. *IEEE Transactions on Magnetics*, **40** (4), 2994–2996 (2004)